Effect of clay content on the thermal conductivity of unfrozen and frozen sandy soils

Quoc Hung Vu, Jean-Michel Pereira, Anh Minh Tang

Effect of clay content on the thermal conductivity of unfrozen and frozen sandy soils

Quoc Hung VU, Jean-Michel PEREIRA, Anh Minh TANG

Navier, Ecole des Ponts, Univ Gustave Eiffel, CNRS, Marne-la-Vallée, France

Corresponding author:

Dr. Anh Minh TANG

Director of Research

Ecole des Ponts ParisTech

6-8 avenue Blaise Pascal

77455 Marne-la-Vallée

France

Email: anh-minh.tang@enpc.fr

Abstract: Thermal conductivities of five sandy soils subjected to freezing-thawing and drying-wetting cycles were determined. Specimens were prepared at five different clay contents of 0, 5, 10, 15, 20% prior to compaction at the Proctor maximum dry density. Soil specimens were saturated prior to freezing-thawing and drying-wetting experiments. During a freezing-thawing cycle, soil's thermal conductivity and unfrozen water content were measured at different temperatures ranging from -3 °C to 0 °C. During a drying-wetting cycle, soil's thermal conductivity was measured at different water contents. The experimental results were then compared with predictions by two of the most appropriate existing models, namely De Vries's and Johansen's models, in order to provide insights into the effects of clay content on soil thermal conductivity at (saturated and unsaturated) unfrozen and frozen states.

Keywords: clay content, thermal conductivity, prediction, unsaturated soils, frozen soils.

1. Introduction

Soil thermal conductivity is one of the key parameters for designing the balance and transfer of heat in many areas of engineering. In cold regions, for instance, soils exist in two states: unfrozen and frozen, depending on many factors such as their composition, pressure and particularly environmental condition (Andersland and Ladanyi, 2004; Cui et al., 2020a; Johansson, 2009; Tian et al., 2016; Zhao and Si, 2019). The state change strongly alters soil thermal conductivity (Cui et al., 2020b; Farouki, 1986; Ji et al., 2021) leading to complexity in the prediction of soil thermal conductivity.

In general, thermal conductivity of soils can be measured using two approaches, based either on steady-state or transient-state regimes (He et al., 2021; Zhao et al., 2019). Each approach includes various methods, such as steady-state heat flow meter, steady-state flat plate, transient spherical probe, transient plate source and transient heat pulse (Cui et al., 2020b; Zhao et al., 2019). Within the steady-state approach, thermal conductivity is determined from the proportionality between heat flow and the applied temperature gradient when heat transfer in soil has already reached the steady state. Reversely, within the transient-state approach, a heat input is applied to the tested soil during a certain time and thermal conductivity is determined from the measurement of increasing rate of soil's temperature and the calibration of Fourier's heat transfer law. These methods have been commonly used for measuring thermal conductivity of unfrozen soils. However, their efficiency when applied to frozen soils is questionable. For steady-state methods, a temperature gradient across a soil specimen can result in water redistribution and ice melting. These problems were also found in application of transient-state methods but with smaller impact because small heat input can be considered (He et al., 2021; Yan et al., 2019).

Various studies investigated the effects of several parameters on thermal conductivity of unfrozen soils such as temperature (Sepaskhah and Boersma, 1979; Tarnawski and Leong, 2000), water content (Abu-Hamdeh, 2003; Nguyen et al., 2017; Smits et al., 2010), dry density (Abu-Hamdeh, 2003; Tang et al., 2008), salinity (Abu-Hamdeh and Reeder, 2000), mineralogy (Bristow, 1998; Côté and Konrad, 2005b) and fines content (Zhang et al., 2017, 2015). These effects are directly related not only to thermal properties of each component but also to the arrangement of soil particles.

A significant effort in measurement of thermal conductivity of frozen soil has been made, particularly, over recent years (Kersten, 1949; Lu et al., 2018; Penner, 1970; Tian et al., 2017; Zhang et al., 2018). These studies also demonstrated the effects of various parameters on thermal conductivity of frozen soils. The presence of ice (replacing water) changes thermal properties of components (2.2 W/(m.K) for ice and 0.57 W/(m.K) for liquid water) and also in arrangement of grain particles (ice segregation). Consequently, the ratio between ice and unfrozen water strongly affects the heat conduction in soils. In addition to temperature, the amount of unfrozen water or ice in frozen soils also depends considerably on the nature of fine particles and their fraction (Li et al., 2020; Tian et al., 2014; Tice et al., 1976; Zhang et al., 2020).

Since several parameters can affect the thermal conductivity of soils, the prediction of the thermal conductivity requires adequate models, able to represent this complexity. For unfrozen soils, many models, developed over the past decades, have shown their efficiency (De Vries, 1963; Farouki, 1986; Johansen, 1977; Kersten, 1949; Mickley, 1951). In particular, by reviewing and evaluating 14 models applied to 62 sands from 20 studies, recently Wang et al. (2020) found that the models of Chen (2008) and Zhang et al. (2017) are the most accurate for thermal conductivity of unfrozen sands over the full range of water content. Unfrozen

soils models were also applied for predicting thermal conductivity of frozen soils (Côté and Konrad, 2005a; Johansen, 1977; Tian et al., 2016). By reviewing and evaluating 39 thermal conductivity models for frozen soils, recently He et al. (2021) identified four best models corresponding to four categories consisting of linear/non-linear regression model, physical model, mixing model and normalized thermal conductivity model. However, none of these models could prove a high prediction accuracy. The occurrence of ice at decreasing temperature indeed complicates the role played by soil components (content and distribution) on soil thermal conductivity.

Among various parameters, fine particles play an important role in filling the pores between coarse grains and also in increasing surface contact between coarse grains. Depending on the nature of each type of fine particles, their impact on thermal conductivity of soil varies. In the study of Zhang et al. (2015) with pure quartz sand, thermal conductivity of sands was increased to a peak value by increasing the fines content to a critical value. However, the critical fines content depends on the mean grain size ratio of fines to coarse grains, the grain shape and also moisture state. Additionally, in the case of clay-sand mixture, Zhang et al. (2017) showed lower values of critical clay content.

Measurements of thermal conductivity were also performed on different types of frozen soils (He et al., 2021; Tian et al., 2016). Kersten (1949) conducted thermal conductivity measurements on 19 soils at various densities, water contents and negative temperatures (-28 °C, -18 °C and -4 °C). These 19 studied soils are very diverse in terms of grain size, from clay to gravel. The study showed a higher range and a lower range of thermal conductivity corresponding to sandy soils and clayey soils, respectively. Penner (1970) studied thermal conductivity of two clays at temperatures between 0 °C and -22 °C. Afterwards, Penner et al. (1975) also studied 10 other natural soils of different grain sizes at -5 °C and -15 °C. These

two studies showed that, in the high-water content range, thermal conductivity of soils increases with increasing grain size at frozen state. Recently, Tian et al. (2016) showed measurements on five soils consisting in loams, clays and sands at -10 °C. The measurements were combined with data of previous studies to elaborate a simplified de Vries-based model for better prediction. In addition, Lu et al. (2018) specifically studied thermal conductivity of one aeolian sand at -15 °C. In general, these previous studies mainly focused on the effects of dry density or water content on thermal conductivity of frozen soils. Consequently, no experimental study has been conducted on the effects of clay content on frozen soils. However, clay content would modify the microstructure of sandy soils and its hydro-thermal behaviour such as soil freezing characteristic curve (Vu et al., 2022).

The present study aims at systematically investigating the effect of clay content on thermal conductivity of unfrozen and frozen sandy soils in two series of experiments corresponding to freezing-thawing and drying-wetting tests. Clean sand was mixed with clay to obtain sandy soils with clay content of 0, 5, 10, 15, and 20% by dry weight prior to compaction at the Proctor maximum dry density followed by a saturation stage. For freezing-thawing process, soil's thermal conductivity and unfrozen water content were measured at different soil's temperatures (ranging from -3 °C to 0 °C) during a freezing-thawing cycle. In parallel, measurement of soil thermal conductivity during a drying-wetting cycle was performed on the same materials. Finally, the performance of two of the most appropriate models (after a recent review) in predicting the obtained experimental results was assessed in order to provide in-depth understanding of the heat conduction process in unfrozen and frozen soils within various clay contents.

2. Materials and experimental method

2.1. Material

Fontainebleau sand (97-99% quartz) and Speswhite Kaolin clay, whose physical properties determined by Boussaid (2005) are shown in Table 1, were mixed with distilled water to obtain optimum water content determined from Standard Proctor compaction (ASTM, 2021) curves obtained on the same soils. Prior to compaction in a rigid metallic cylindrical cell (150 mm in height and 150 mm in diameter) to reach the predetermined density, the wet soils were packed in a plastic bag for at least 24 h for moisture distribution homogenisation. Fig. 1 presents the grain size distribution of the investigated soils (the name of each soil corresponds to its clay content: for instance, S10 corresponds to a soil having 10% of clay and 90% of sand in dry mass). Table 2 shows physical properties of specimens in two experiments: freezing-thawing (noted by T1) and drying-wetting (noted by D1). The dry density of the samples shown in Table 2 is close to the maximum dry density of the corresponding sand-clay mixture. Water content at compaction was taken equal to the optimum water content determined by Boussaid (2005). It is worth noting that optimum water contents for intermediate fines content (5% and 15%) have been interpolated from the available data.

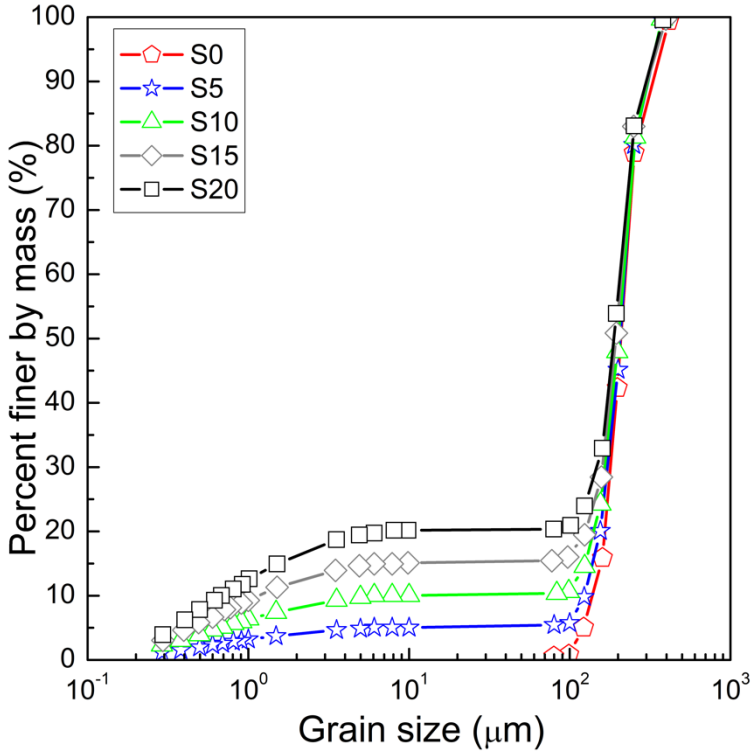

144

145 Fig. 1. Grain size distribution curves.

146 Table 1. Physical properties of Speswhite Kaolin clay and Fontainebleau sand (Boussaid,

147 2005).

Properties	**Speswhite Kaolin clay**	**Fontainebleau sand**
Median grain size, D_{50} (mm)	-	0.21
Uniformity coefficient, C_U	-	1.52
Minimum void ratio, e_{min}	-	0.54
Maximum void ratio, e_{max}	-	0.94
Particle density, ρ_s (Mg/m^3)	2.65	2.65
Minimum dry density, $\rho_{d,min}$ (Mg/m^3)	-	1.37
Maximum dry density, $\rho_{d,max}$ (Mg/m^3)	1.45	1.72
Liquid limit, LL (%)	55	-

Plastic limit, PL (%)	30	-
Plasticity index, PI	25	-
Specific surface area (m^2/g)	0.94	-
Particle diameter < 0.002 mm (%)	79	-
Particle diameter > 0.01 mm (%)	0.5	-

148 Table 2. Physical properties of soils in freezing-thawing (T1) and drying-wetting (D1)
149 experiments.

Test No.	**Clay content (%)**	**Water content at compaction (%)**	**Dry density (Mg/m^3)**	**Porosity (-)**
S20-T1	20	11.2	1.98	0.25
S15-T1	15	9.1	1.99	0.25
S10-T1	10	8.0	1.91	0.28
S5-T1	5	7.0	1.78	0.33
S0-T1	0	5.6	1.67	0.37
S20-D1	20	11.2	1.96	0.26
S15-D1	15	9.1	1.99	0.25
S10-D1	10	8.0	1.93	0.27
S5-D1	5	7.0	1.77	0.33
S0-D1	0	-	1.61	0.39

150 **2.2. Setup and procedure for freezing-thawing experiments**

151 The experimental setup used for freezing-thawing experiments is shown in Fig. 2. The sensors
152 used in the freezing-thawing experiments are shown in Table 3. Soil temperature was

measured with a PT100 sensor, soil thermal conductivity was measured with a KD2-Pro (RK-1) probe and soil volumetric water content was measured with a ML2x Thetaprobe sensor. Two empirical equations due to (1) Smith and Tice (1988) and (2) Topp et al. (1980) were used to infer soil volumetric water content from apparent dielectric constant for frozen and unfrozen soil, respectively:

$$\theta_u = -0.1458 + 3.868 \times 10^{-2} \times K_a - 8.502 \times 10^{-4} \times K_a^2 + 9.92 \times 10^{-6} \times K_a^3 \quad (1)$$

$$\theta_u = -5.3 \times 10^{-2} + 2.92 \times 10^{-2} \times K_a - 5.5 \times 10^{-4} \times K_a^2 + 4.3 \times 10^{-6} \times K_a^3 \quad (2)$$

where K_a is the apparent dielectric constant and θ_u is the unfrozen volumetric water content.

After compacting the soil specimen in the cylindrical cell at optimum water content to the desired dry density (Table 2) using Standard Proctor compaction procedure, the sensors were inserted into the soil as shown in Fig 2. Afterwards, an expanded polystyrene layer was placed to cover the soil specimen for heat insulation purposes. The soil specimen was then saturated by injecting water from its bottom (for 0.5 to 2 days depending on clay content) until a 10 mm layer of water is visible on the top of the specimen. Afterwards, the cell containing the soil specimen was immersed in a temperature-controlled bath (F38-EH JULABO with ±0.03 °C accuracy), as shown in Fig. 2, to start the freezing-thawing experiment. The bath temperature was first set at a temperature between 0 °C and -1 °C (slightly higher than the expected temperature of spontaneous ice nucleation). After the temperature stabilised at this initial state, it was then decreased in steps of 0.1 °C to freeze the soil pore water. Once freezing was triggered (most of the liquid water was transformed into ice), the temperature was decreased in steps of 0.2 °C until -2 °C or -3 °C to determine the change in thermal conductivity and liquid water content upon further cooling. Afterwards, during the heating path, the bath temperature was increased in steps of 0.2 °C to 0 °C in order

to thaw the frozen soil. During both cooling and heating paths, after the equilibrium was reached at each step, the thermal conductivity was measured at least three times with a 1-hour interval between two consecutive measurements to verify the equilibration of soil's temperature and unfrozen water content. The equilibrium state was considered reached when changes (during 2 h) in the soil temperature and volumetric unfrozen water content (measured by the sensors) were negligible (< 0.05 °C for temperature and < 1% for water content). Data from the tensiometer, providing cryo-suction developing when the freezing process is triggered, were not analysed because they are out of the scope of this paper.

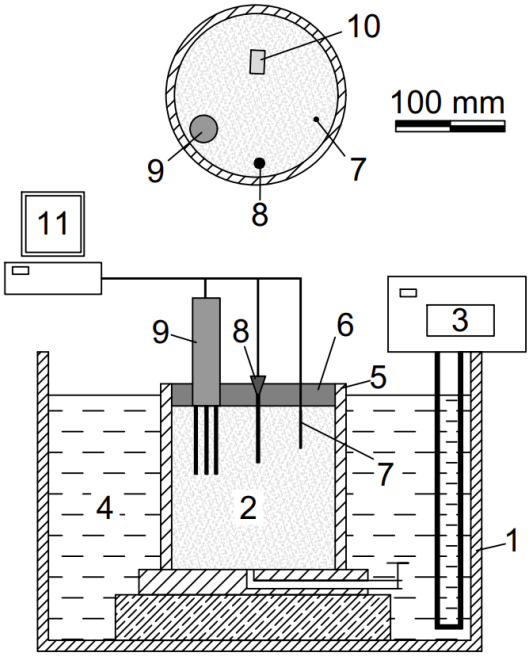

Fig. 2. Setup for freezing-thawing experiments: (1) Temperature-controlled bath; (2) Soil specimen; (3) Temperature control system; (4) Heat transfer liquid (30% ethylene glycol + 70% water); (5) Metallic cylindrical cell; (6) Insulating cover; (7) Temperature sensor; (8) Tensiometer; (9) Soil water content sensor; (10) Thermal conductivity probe; (11) Data

187 logging system. A bar representing a scale of 100 mm is shown to illustrate the setup
188 dimensions.

189 Table 3. Properties of sensors used in freezing-thawing and drying-wetting experiments.

Measured parameters	Principle	Type	Supplier	Accuracy	Range
Temperature (Freezing-Thawing test)	Resistance temperature detector	PT100	Mersurex	±0.03 °C	- 200 to 400 °C
Volumetric water content (both tests)	Time domain reflectometry (dielectric permittivity)	ThetaProbe ML2x (4 rods)	AT Delta-T service	0.01 m^3/m^3	0.01 to 1 m^3/m^3
Suction (Freezing-Thawing test)	Tensiometer	T5x	Meter Group	±0.5 kPa	-160 to 100 kPa
Thermal conductivity (both tests)	Transient line heat source	KD2-Pro (RK-1)	Meter Group	10% of measured value	0.1 to 4 W/(m.K)
Suction (Drying-wetting test)	Tensiometer	T8	Sol Mesures	±0.5 kPa	-100 to 100 kPa

190

191 **2.3. Setup and procedure for drying-wetting experiments**

192 The drying-wetting experiments conducted in this study followed a similar methodology to
193 that described by Nguyen et al (2017). The sensors and experimental setup are shown in Table
194 3 and Fig. 3. A thermal conductivity sensor KD2-Pro (TR-1) was installed in the centre of the
195 specimen while two other sensors including water content sensor and tensiometer were
196 installed close to the cell wall. This configuration minimizes the effect of these two sensors on
197 the thermal conductivity sensor. The empirical equation (2) due to Topp et al. (1980) was also
198 used to infer volumetric water content from apparent dielectric constant for soils during
199 drying-wetting processes. Data from the tensiometer, providing suction developed during the
200 initial drying, were not analysed because they are out of the scope of this paper.

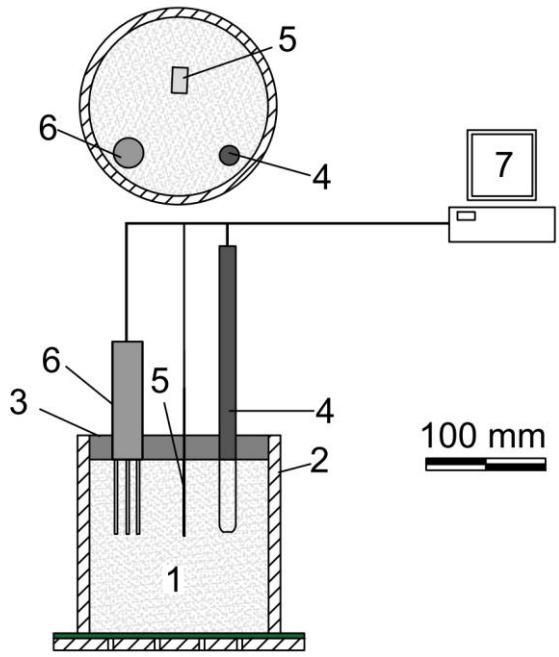

Fig. 3. Setup for drying-wetting experiments: (1) Soil; (2) Metallic cylindrical cell; (3) Insulating cover; (4) Tensiometer; (5) Thermal conductivity probe; (6) Soil water content sensor; (7) Data logging system. A bar representing a scale of 100 mm is shown to illustrate the setup dimensions.

After compaction and saturation, the soil specimen was first subjected to a drying path in steps. For this purpose, two holes (50 mm in diameter) were created on the top cover allowing soil water to evaporate. For each drying step, the two holes were opened to allow evaporation from the top surface. A fan was put next to the specimen to increase the evaporation rate. After a certain duration, the two holes were covered by two lids to avoid moisture exchange with the atmosphere. The equilibrium moisture was reached after several hours. Moisture equilibrium was tracked by volumetric water content and suction sensors. When water evaporation took place, the measured suction increased quickly and the measured water content decreased quickly. During the equilibrium phase, suction decreased and water content increased slowly to reach equilibrium. Similar phenomena have been observed in Nguyen et

al. (2017). Thermal conductivity measurements were performed at equilibrium prior to the subsequent drying step.

After the drying path, the soil specimen was also subjected to a wetting path in steps. For each step, a small quantity of water was added through the two holes on the top cover, which were then closed for several hours to ensure that water was redistributed homogeneously within the specimen.

The homogeneity of water distribution (equilibrium state), during both drying and wetting paths, was assumed to be reached when changes in soil suction and soil volumetric water content during a 1-hour period were negligible (< 1 kPa for suction and < 1% for water content). At the end of each step, soil thermal conductivity was measured three times with a 1-hour interval between two consecutive measurements.

3. Experimental results

3.1. Thermal conductivity of frozen soil

As an example of a freezing-thawing test, the results of test S10-T1 are shown in Fig. 4, where soil temperature (T), volumetric unfrozen water content (θ_w) and thermal conductivity (λ) are plotted versus elapsed time. Initially, T was imposed at -1.2 °C without inducing freezing (formation of ice). A cooling path was first applied by decreasing T in steps of 0.1 °C. During the period where T remained higher than -1.6 °C, T was controlled through the bath's temperature, θ_w and λ remained constant. At 77 h (when T was imposed at -1.6 °C), freezing process occurred showing an abrupt increase of T to -0.1 °C prior to a progressive decrease to reach the imposed temperature (-1.6 °C) again. At this time, θ_w decreased to 3% (because of the formation of ice) while λ increased from 4 W/(m.K) to 5 W/(m.K). After this

first formation of ice, T was further decreased in steps of -0.2 °C from -1.7 °C to -2.9 °C. λ increased while θ_w slightly decreased during this further cooling path. When T reached -2.9 °C, a heating path was imposed in steps of 0.2 °C. During this path, θ_w increased progressively while λ decreased. It is noted that the two particularly high values of λ at 400 h and 560 h were observed but they were not considered as reliable values due to the effect of latent heat on measurement. Actually, during the measurement by the linear heat source method, a constant heat power was supplied and slightly heated the probe. Thermal conductivity was estimated by the rate of probe's temperature increase with the logarithm of time. When measurements were performed close to the freezing temperature, this heating would induce water thawing in the vicinity of the probe. This thawing required heat (latent heat) and reduced the probe's temperature (inducing an overestimation of thermal conductivity). These measurements are thus not presented in the following figures.

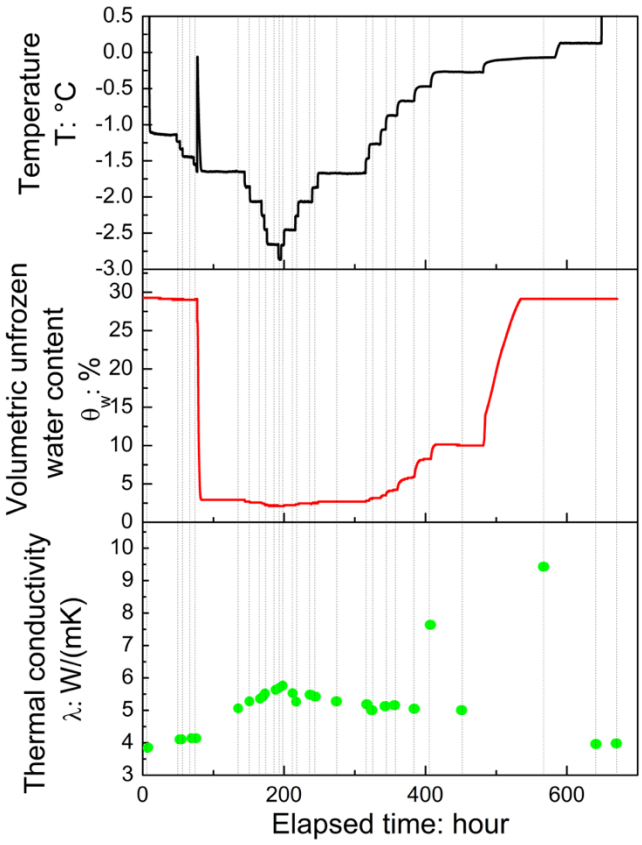

Fig. 4. Time evolution of temperature, unfrozen volumetric water content and thermal conductivity during test S10-T1.

Fig. 5 shows, for test S10-T1, the relationships between T, λ, and θ_w obtained at the end of each step included in a freezing path and a subsequent thawing path (the considered equilibrium state corresponds to the vertical dotted lines shown in Fig. 4). During the cooling path (dark line), as shown in Fig. 5*a*, freezing occurred when T reached -1.6 °C, inducing a sudden decrease of θ_w from 28% to 3%. When T continued to decrease to -2.9 °C, θ_w decreased slightly to 2%. During the heating path (red line), thawing occurred progressively inducing an increase of θ_w. The relationship between θ_w and T is similar between the cooling and the heating paths, except for the period before the occurrence of freezing. Similar conclusions can be observed on the relationship between λ and T (Fig. 5*b*). However, a unique relationship can be observed between λ and θ_w (Fig. 5*c*).

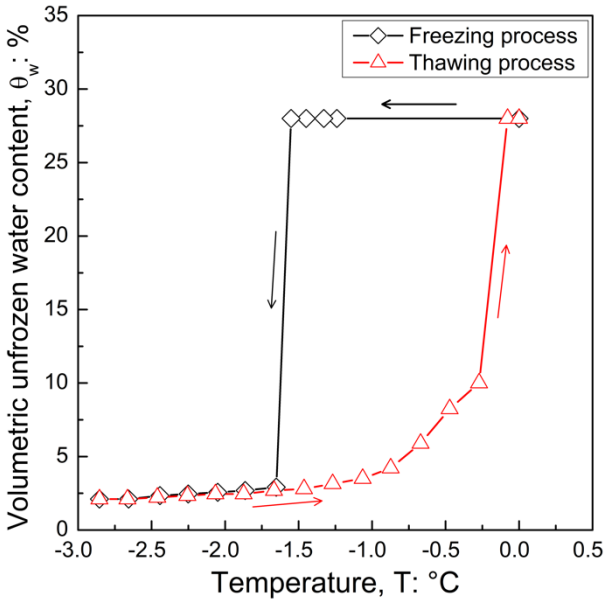

(a)

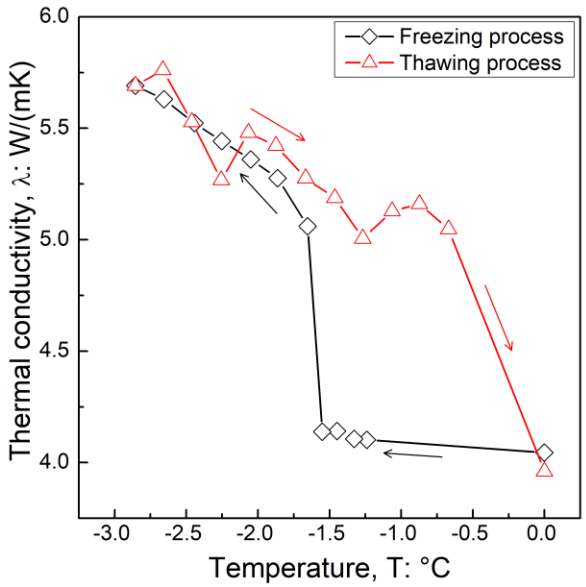

(b)

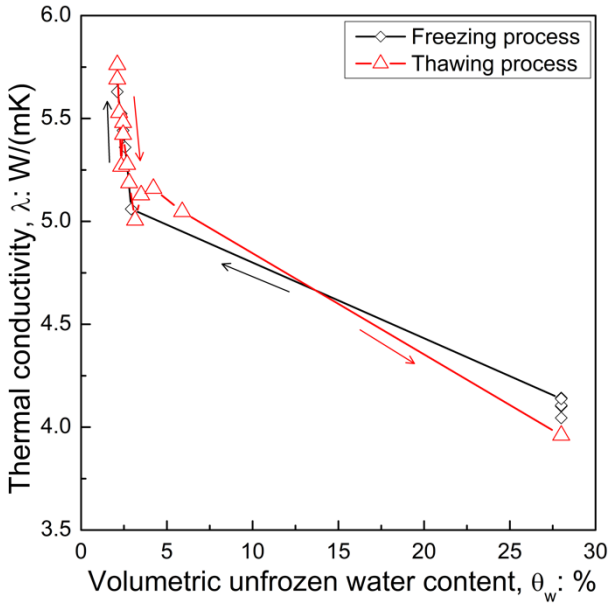

(c)

263 Fig. 5. Relationships between (a) volumetric unfrozen water content and temperature, (b)
264 thermal conductivity and temperature, (c) thermal conductivity and volumetric unfrozen water
265 content of test S10-T1.

Detailed analyses of the relationship between volumetric unfrozen water content and temperature (soil freezing characteristic curve) obtained for all soils were presented in Vu et al. (2022). In the present work, results on thermal conductivity are further analysed.

Fig. 6 presents the results of all the freezing-thawing experiments where λ is plotted versus T. It can be observed that all these results show similar trends. During the initial cooling, λ did not change when T decreased. λ increased abruptly when freezing occurred. Afterwards, the relationship between these two quantities were similar on the freezing and thawing paths. Generally, λ was higher at a lower T.

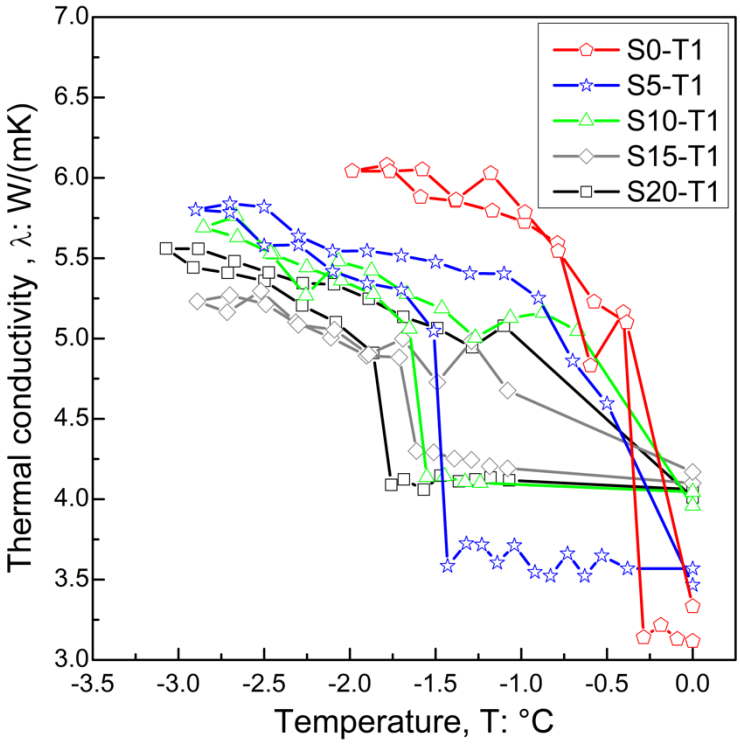

Fig. 6. Thermal conductivity versus temperature for all freezing-thawing experiments.

Fig. 7 presents the results of all specimens at frozen state where λ is plotted versus θ_w and T. It can be observed that all these results show a reversible behaviour of λ at frozen state, particularly with θ_w. λ increased significantly with decreasing θ_w in the range of low values

279 of unfrozen water content. In addition, to provide the same thermal conductivity, volumetric
280 unfrozen water content has to be higher for a higher clay content. Otherwise, as shown in Fig.
281 7b, at the same temperature in frozen state, adding fines (from 0% to 15%) decreases λ
282 significantly.

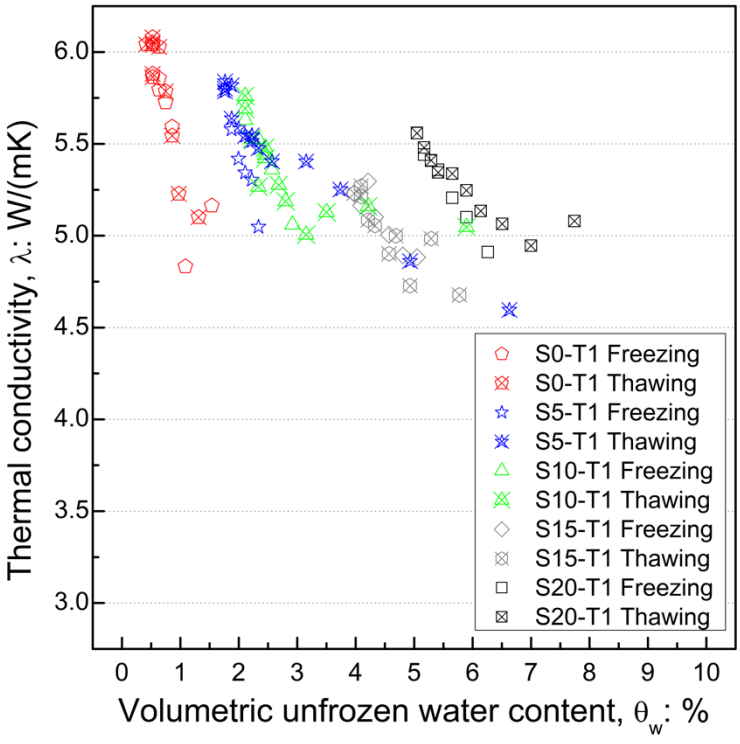

283

284 (a)

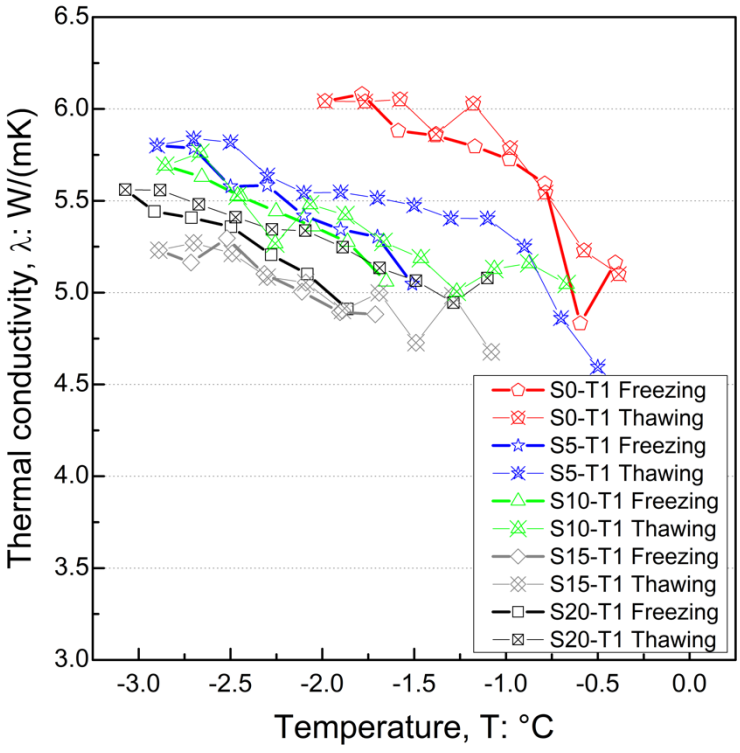

285

286 (b)

287 Fig. 7. Thermal conductivity versus (a) volumetric unfrozen water content and (b)
288 temperature for all freezing-thawing experiments.

289 Fig. 8 presents thermal conductivity versus water degree of saturation (S_w) only for soils at
290 frozen state. Generally, λ was higher at a lower value of S_w. Beside the experimental results,
291 results obtained by models' prediction are also plotted for comparison in this figure (see
292 section 4).

293

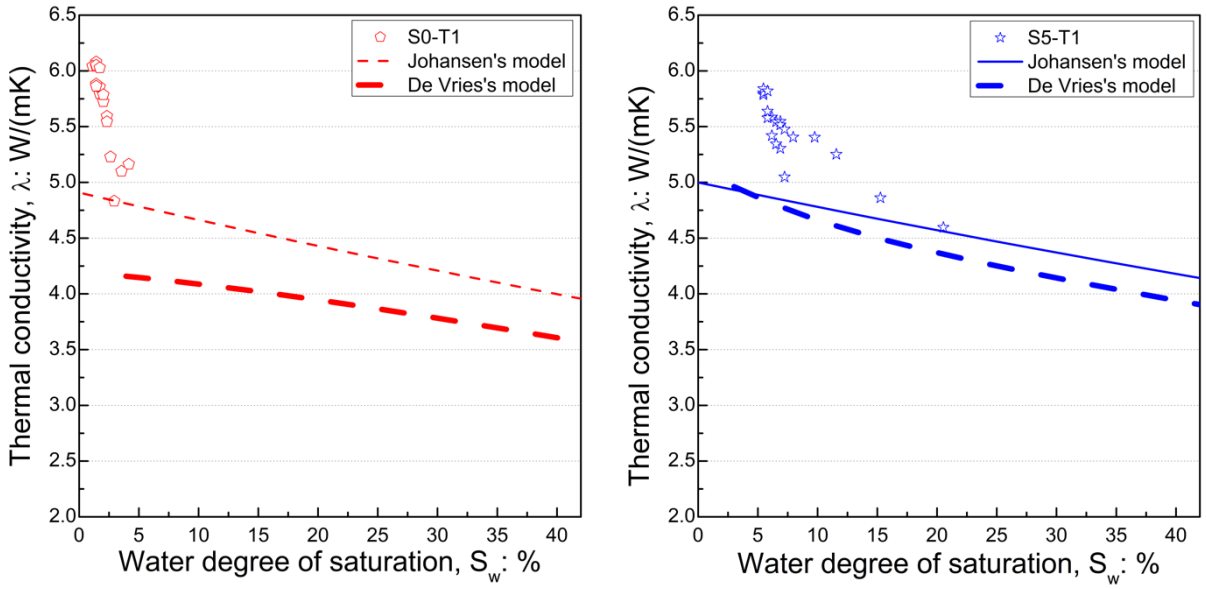

(a) (b)

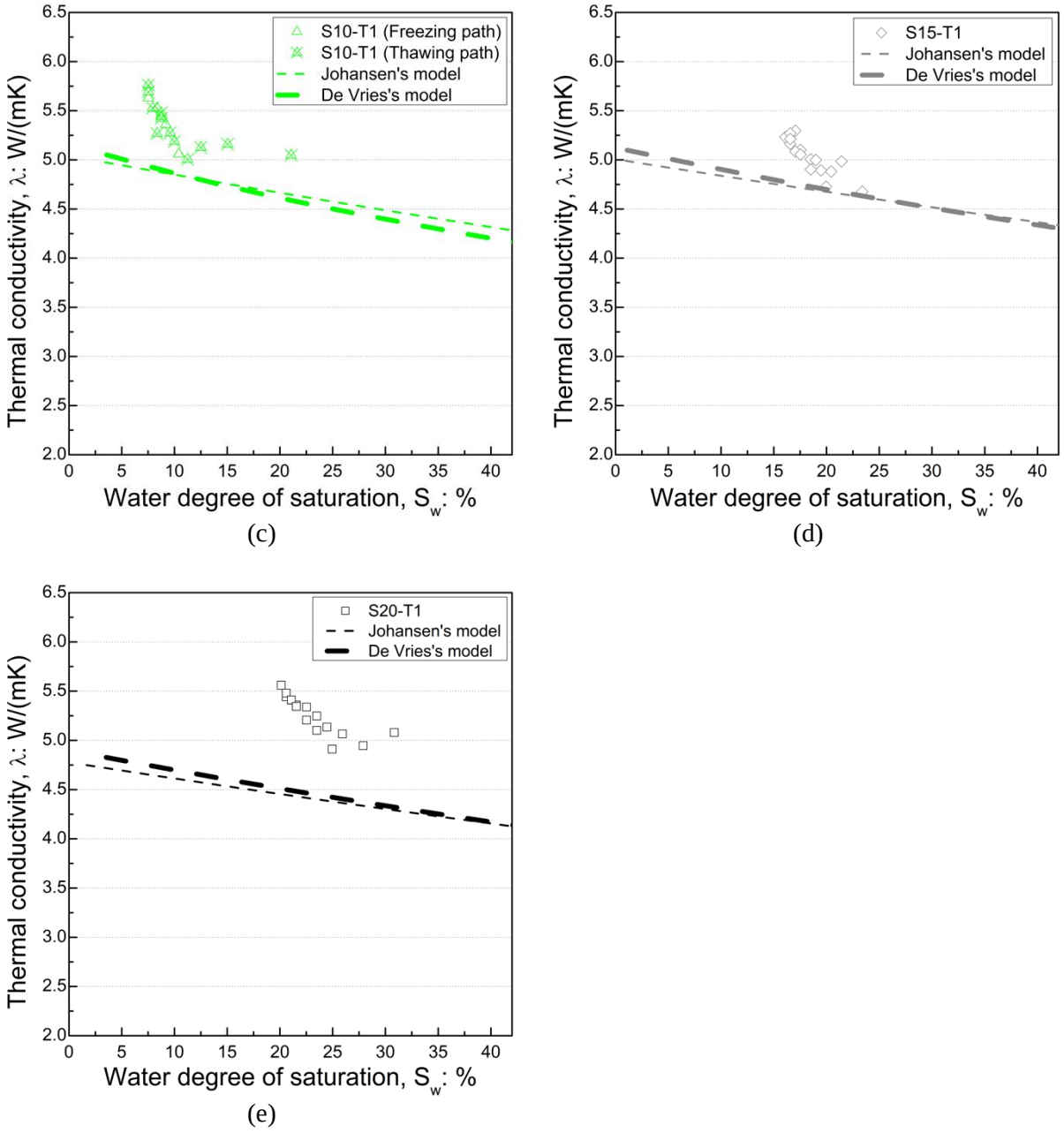

294 Fig. 8. Experimental results and models' prediction for thermal conductivity versus water
295 degree of saturation for frozen soils: (a) S0-T1; (b) S05-T1; (c) S10-T1; (d) S15-T1; (e) S20-
296 T1.

297 **3.2. Thermal conductivity of unfrozen soil**

298 Fig. 9 shows the evolution of θ_w and λ versus time for test S10-D1. From the beginning to
299 650 h, the specimen was subjected to various drying steps prior to be subjected to further
300 wetting steps until 1000 h. From the initial state with θ_w = 25.3%, water evaporation takes
301 place when removing the two lids and θ_w decreased slowly. After several hours, covering the
302 holes with the lids again prevented water evaporation. θ_w continued to decrease with lower
303 rate prior to stabilizing in further hours at 21.6% and measurement of λ was then conducted.
304 Such drying step was repeated 8 times until θ_w= 14.2% prior to wetting path. From 650 h,
305 first addition of water in two holes induced a slow increase of θ_w, which stabilized at 15%.
306 The measurement of λ was then also performed prior to the second water addition. In the
307 subsequent wetting steps, adding water induced an abrupt and immediate increase of θ_w,
308 which decreased afterward with slow rate prior to stabilizing. The wetting path was stopped at
309 θ_w = 22.3%.

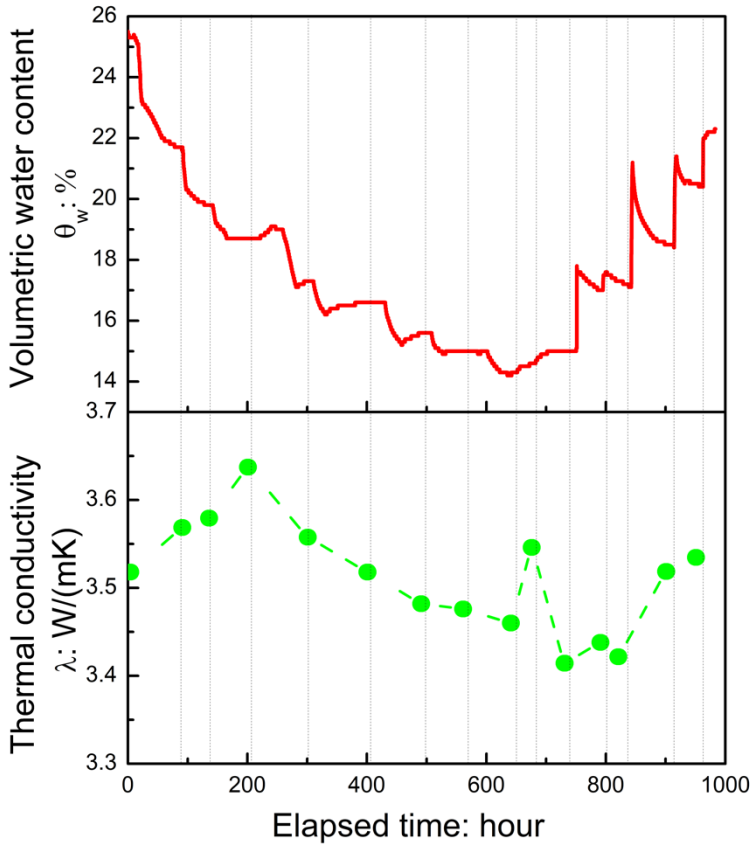

310

311 Fig. 9. Volumetric water content and thermal conductivity of unfrozen soils in wetting-drying

312 process of S10-D1.

Fig. 10 shows the relationship between λ and water degree of saturation (S_w) for all drying-wetting experiments. S_w was calculated from θ_w and soil porosity (n). In this figure, S_w was plotted instead of θ_w in order to facilitate the comparison with data taken from existing studies. Measurements of thermal conductivity of pure sand in drying-wetting experiment (S0-D1) were not conducted and available data found from the literature (Vieira et al., 2019) were used. The results show that adding fines (from 0% to 15%) increased significantly λ

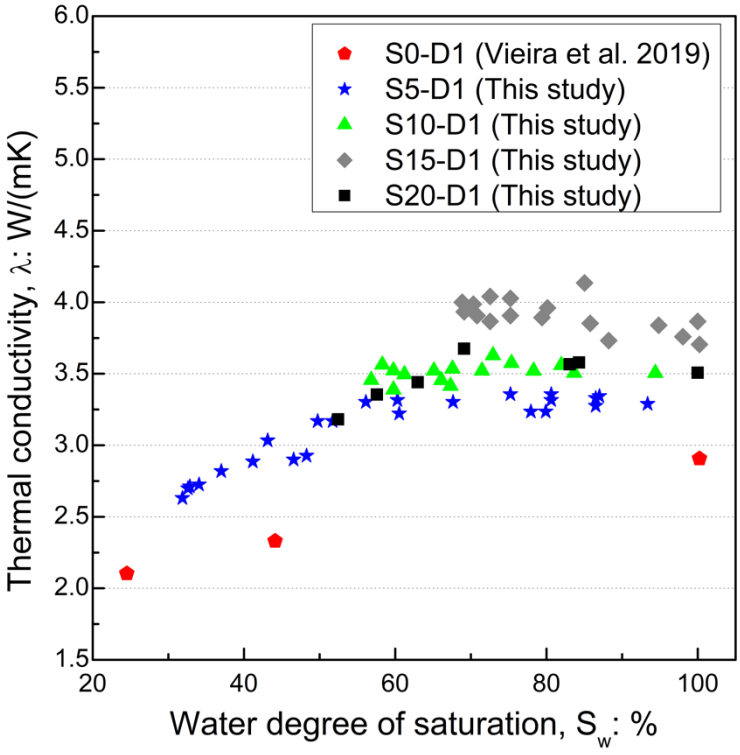

Fig. 10. Thermal conductivity versus water degree of saturation for all drying-wetting experiments.

Fig. 11 shows predictions of models. Zhang et al. (2017) presented data obtained on sand-kaolin mixtures (having similar clay content) compacted at various porosities and degrees of saturation. The sand used in the work of Zhang et al. (2017) was Ottawa-type silica sands (pure sand with more than 99% quartz content). These results are also plotted in Fig. 11.

Results obtained by models' prediction are described in Section 4. All the results showed a strong correlation between λ and S_w for a given porosity (a higher λ was generally obtained at a higher S_w). It is noted that, above S_w = 60%, thermal conductivity remained constant for all soils. Results on pure sand (Fig. 11a) showed that the relationship between λ and S_w was independent of the porosity. For sand-clay mixture, at a given S_w, a higher λ was generally obtained at a lower porosity (Fig. 11*b*,*c*,*e*). Zhang et al. (2017) did not perform tests on mixture with clay content of 15% (Fig. 11*d*). The results obtained in the present work correspond to the range of high degree of saturation (from 50 % to 100%), this range was not

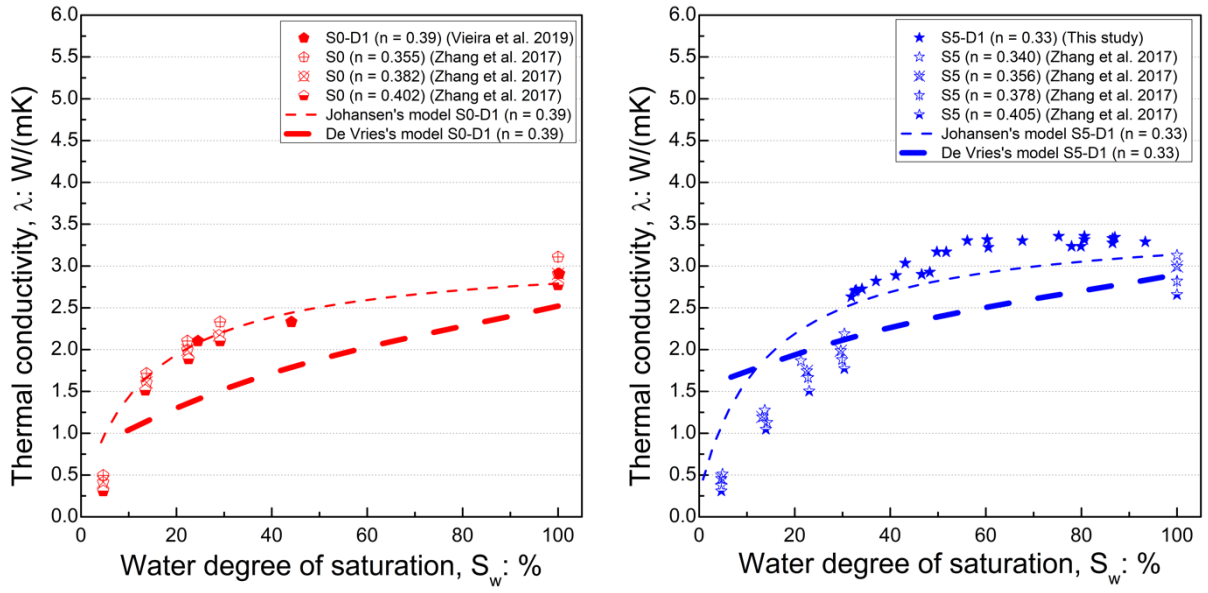

(a) (b)

investigated in the work of Zhang et al. (2017).

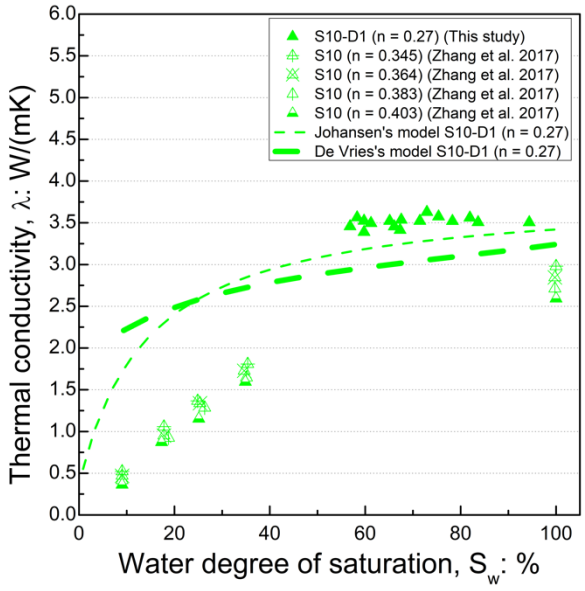

(c)

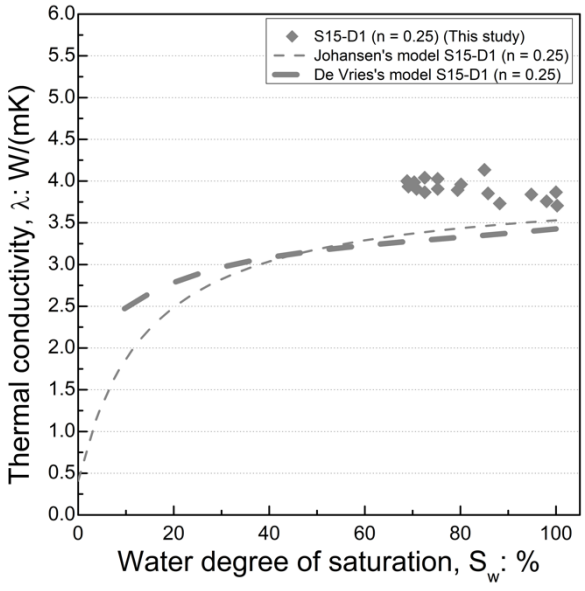

(d)

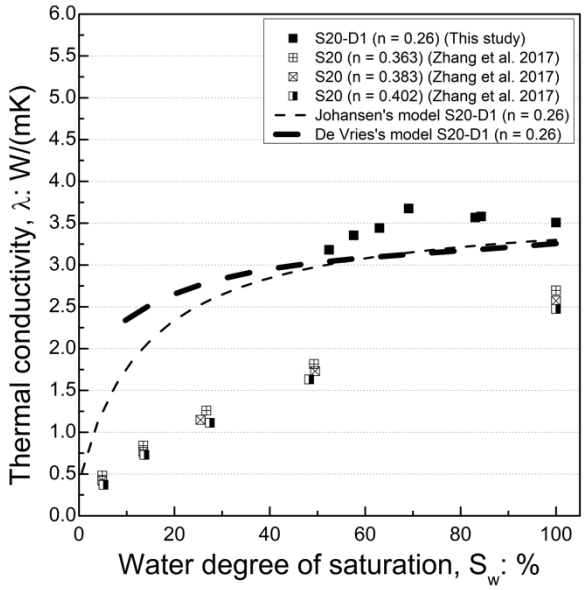

(e)

335 Fig. 11. Experimental results (obtained in this study and that of Zhang et al. 2017) and models
336 prediction for thermal conductivity versus water degree of saturation for unfrozen soils: (a)
337 S0; (b) S5; (c) S10; (d) S15; (e) S20.

338 ## 4. Prediction of soil thermal conductivity

Based on the recent review of He et al. (2021) on 39 models to predict thermal conductivity of frozen soils, two appropriate models were chosen in this study, namely De Vries's model (De Vries, 1963) and Johansen's model (Johansen, 1977). Actually, these models can be used for both frozen and unfrozen soils. They can consider the change in unfrozen water content in frozen soil with temperature change and the effect of clay content.

For the prediction of thermal conductivity of unfrozen and frozen soil in this study, frozen soil was considered as a medium made of four components: unfrozen water, ice, sand and clay, whose volumes are noted as V_w, V_i, V_s, V_c, respectively while unfrozen soil was also considered as a medium made of four components: water, air, sand and clay, whose volumes are noted as V_w, V_a, V_s, V_c, respectively.. The thermal conductivity of water (λ_w) was taken equal to 0.57 W/(m.K) while those of ice (λ_i) and air were taken equal to 2.28 W/(m.K) and 0.025 W/(m.K), respectively (Farouki, 1986). For the soil particles, the thermal conductivity of kaolin (λ_c) was taken equal to 2.44 W/(m.K) while that of sand (λ_s) equal to 7.70 W/(m.K) (Tarnawski et al., 2015).

4.1. De Vries's model

The De Vries's model was extended for predicting thermal conductivity of frozen soil (Farouki, 1986; Tian et al., 2016). In the review of He et al. (2021), the simplified De Vries-based model with the considered shape factors was proved as the best among physical models (Tian et al., 2016). In this study, for better fitting experimental data, De Vries's model is applied considering that ice and sand particles are components immersed in the continuous medium (fluid) that contains water and clay particles, as shown in Fig. 12. The thermal conductivity of frozen soil is then expressed as:

(3) $$\lambda = \frac{\left(\frac{V_f}{V}\right)\lambda_f + F_i\left(\frac{V_i}{V}\right)\lambda_i + F_s\left(\frac{V_s}{V}\right)\lambda_s}{\frac{V_f}{V} + F_i(\frac{V_i}{V}) + F_s(\frac{V_s}{V})}$$

361 Where F_s, F_i are the weighting factors depending on the shape and the orientation of sand and
362 ice particles, respectively. Considering ellipsoidal shape for ice and sand particles, the
363 weighting factor F_n (with $n = \{s, i\}$) is given from shape factor g_a as follows:

(4) $$F_n = \frac{1}{3}\left\{\frac{2}{1 + \left(\frac{\lambda_n}{\lambda_f} - 1\right)g_a} + \frac{1}{1 + \left(\frac{\lambda_n}{\lambda_f} - 1\right)(1 - 2g_a)}\right\}$$

364 with $g_{a(sand)} = 0.182$ (Tarnawski and Wagner, 1992) and

(5) $$g_{a(ice)} = 0.333\left(1 - \frac{\theta_{ice}}{n}\right)$$

365 where, n is the porosity of soil, θ_{ice} is the ice content. The fluid mixture (water and clay
366 particles) properties are given by:

(6) $$\lambda_f = \lambda_w^{\frac{V_w}{V_w+V_c}}\lambda_c^{\frac{V_c}{V_w+V_c}}$$

(7) $$V_f = V_w + V_c$$

367 and the total volume is:

(8) $$V = V_w + V_i + V_s + V_c$$

The De Vries's model was also used to predict thermal conductivity of unfrozen soils in drying-wetting process. In this case, unfrozen soil is composed of sand, air immersed in liquid (mixture of clay and water). The thermal conductivity of unfrozen soil is expressed as:

$$\lambda = \frac{\left(\frac{V_f}{V}\right)\lambda_f + F_a\left(\frac{V_a}{V}\right)\lambda_a + F_s\left(\frac{V_s}{V}\right)\lambda_s}{\frac{V_f}{V} + F_a(\frac{V_a}{V}) + F_s(\frac{V_s}{V})} \quad (9)$$

The weighting factors F_s, F_a are similar to the previous expression with the shape factor below:

$$g_{a(air)} = 0.333 - \frac{\theta_{air}}{n}(0.333 - 0.035) \quad (10)$$

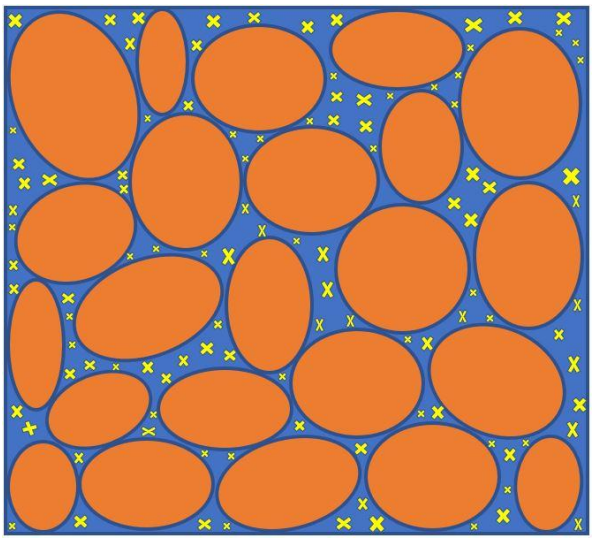

(a)

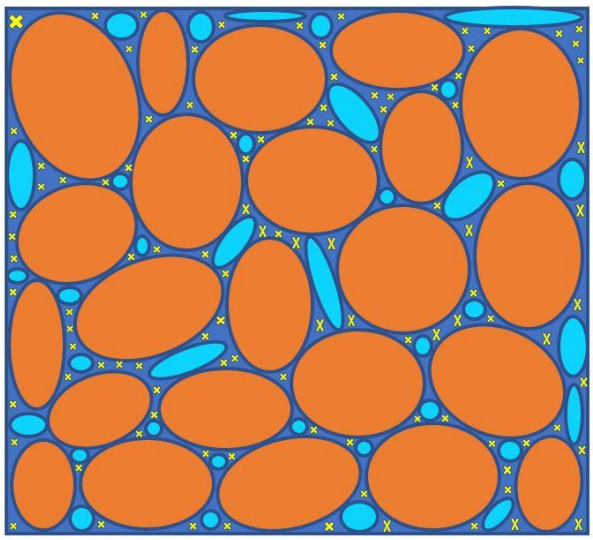

(b)

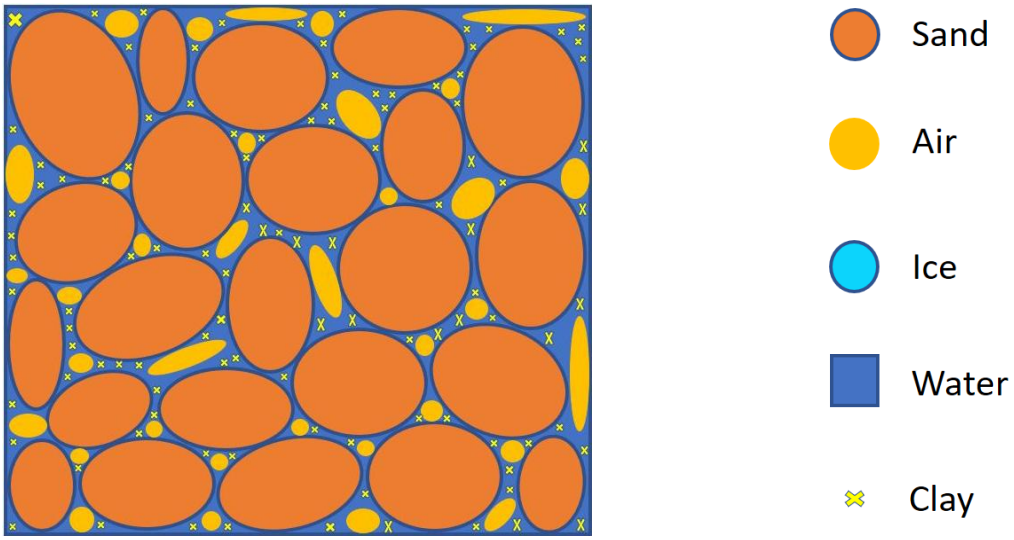

(c)

373 Fig. 12. Schematic view of soil media in (a) unfrozen saturated state, (b) frozen saturated state
374 and (c) unfrozen unsaturated state.

375 The comparison (Fig. 8) showed that the De Vries's model underestimated measured values
376 of λ of all frozen soils. The model also showed a higher λ at a lower S_w but could not capture
377 the strong effect of S_w when this later is small. For unfrozen soils (Fig. 11), the De Vries'
378 model also showed a higher λ at a higher S_w but could not capture accurately the relationship
379 between these two parameters for the whole range of S_w (varying from 0 to 100%).

380 **4.2. Johansen's model**

381 Geometric mean was proposed to calculate the thermal conductivity (λ) of saturated frozen
382 soil by Johansen (Johansen, 1977):

$$\lambda = \lambda_w^{f_w} \lambda_i^{f_i} \lambda_c^{f_c} \lambda_s^{f_s} \quad (11)$$

383 where f_w , f_i , f_c , f_s are volume fraction of water, ice, clay and sand, respectively.

In this study, for unfrozen soils subjected to drying-wetting process, the thermal conductivity introduced by Johansen was expressed as:

$$\lambda = (\lambda_{sat} - \lambda_{dry})K_e + \lambda_{dry} \quad (12)$$

where $\lambda_{sat}, \lambda_{dry}$ are respectively the thermal conductivity in saturated and dry states at the same dry density, K_e is a function representing the influence of water degree of saturation S_w on the thermal conductivity. According to Côté and Konrad (2005a), K_e is proposed as follows:

$$K_e = \frac{\kappa S_w}{1 + (\kappa - 1)S_w} \quad (13)$$

where κ is an empirical parameter accounting for the soil type effect. Zhang et al. (2017) proposed an equation to illustrate the relationship between κ and quartz (sand) content. In this study, $\kappa = 8$ was chosen because it provided the best prediction.

$$\lambda_{dry} = \frac{0.135\rho_d + 64.7}{\rho_s - 0.947\rho_d} \ \mathrm{W/(m.K)} \quad (14)$$

$$\lambda_{sat} = \lambda_w^{f_w}\lambda_c^{f_c}\lambda_s^{f_s} \ \mathrm{W/(m.K)} \quad (15)$$

where the dry unit weight, ρ_d, and the unit weight of the solids, ρ_s, are expressed in kg/m^3.

For frozen soils, compared to De Vries's model, Johansen's model predicted higher values for soils with low clay content (S0-T1, S5-T1, S10-T1) but the improvement was not significant (Fig. 8). For soils with high clay contents, the two models provided similar results.

For unfrozen soils, the modified Johansen's model proposed by Zhang et al. (2017) gave a better prediction compared to the De Vries's model (Fig. 11). It gave better prediction for

soils with low clay contents (S0-D1, S5-D1, S10-D1). However, for soils with high clay contents, the improvement compared to De Vries's model was not significant.

5. Discussion

The measurement of unfrozen water content in the present study was converted from the measurement of the apparent dielectric constant. The latter was calculated from the dielectric constant of each component in soils, particularly water and ice, which are influenced by temperature variation (Haynes, 2016; Wraith and Or, 1999). Several existing models can estimate moisture content from unfrozen soil apparent dielectric constant (Birchak et al., 1974; He and Dyck, 2013; Nagare et al., 2011; Roth et al., 1990; Schafer and Beier, 2020; Smith and Tice, 1988; Stähli and Stadler, 1997; Topp et al., 1980; Watanabe and Wake, 2009). The most used is Topp's empirical model (Topp et al., 1980) but it is not compatible with frozen soils (Smith and Tice, 1988; Spaans and Baker, 1995; Zhou et al., 2014). Otherwise, Smith and Tice (1988) proposed a model based on the comparison of unfrozen water content measured from NMR and TDR methods for 25 soils covering a wide range of specific surface areas. For this reason, in the present work, the model of Smith and Tice (1988), which provides an accuracy of ±3% compared to measurements from NMR method, considered as the reference, was used for frozen soils.

During the freezing process, the volume of specimen would increase, thus modifying the contact between soil and the probes. In the present work, the potential lateral expansion of the specimen is prevented by the rigid metallic cell. The soil/probe contact was thus supposed to be not influenced by the freezing process.

421 The obtained results show that the thermal conductivity of soil (λ) at frozen state is higher
422 than that at unfrozen state. Even if this trend was observed in various existing studies, most of
423 the existing works provide data corresponding to one or few values of negative temperature.
424 Few works provided an almost continuous relationship between λ and soil temperature. In the
425 present work, during the thawing path, the rate of decrease of λ with temperature change for
426 temperature in the range of -3 °C to -1 °C was lower than in the range of -1 °C to 0 °C (Fig.
427 6). Similar trend was observed by Overduin et al. (2006) and Zhang et al. (2018). Such a
428 difference induced by the phase change of water can be explained by the conductivity of ice
429 (λ_i) being approximately four times higher than that of liquid water (λ_w). These values
430 depend significantly on temperature and pressure. However, λ_i (Bonales et al., 2017; Slack,
431 1980) and λ_w (Lawson et al., 1959) can be considered as constants in the relatively small
432 temperature range investigated in the present study. It is believed that the increase of λ after
433 freezing occurrence relates mainly to the small amount of water transforming into ice because
434 there was almost no hysteresis observed in the relationship between λ and θ_w in this range. As
435 illustrated in Fig. 12, ice is mainly formed from water in the centre of the pores. In the case
436 where ice could not contain clay, the decrease of unfrozen water content caused the increase
437 of clay concentration in unfrozen water. It is noted that this latter plays a role as a contact
438 between sand grains. The phenomenon of increasing clay concentration in water contributes
439 considerably to the efficiency of heat conduction because it not only increases the thermal
440 conductivity of the fluid (Kim et al., 2011), but also strengthens heat transfer between sand
441 grains (Johansen, 1977).

442 The two chosen models were not able to predict well the thermal conductivity of frozen sandy
443 soils in this study. For De Vries's model, considering the continuous medium (fluid) as a
444 mixture of water and clay particles with ellipsoidal shape for ice and sand particles could

contribute to the low accuracy of the model. It is noted that in this model, considering λ_i and λ_s as constants, the application of geometric mean for λ_f is consistent with the measurements on saturated kaolinite in the study of Kim et al. (2011). For Johansen's model, geometric mean formula could only consider the thermal conductivity of each component and their fraction. So that small change in f_i and f_w could not induce significant changes in the thermal conductivity of frozen soils. In addition, both models could not properly capture the components arrangement that affects how heat transfers through the clayey sands.

The results obtained on frozen soil show that at the same temperature, thermal conductivity measured on the thawing path was slightly higher than that on the freezing path (Fig. 6 and Fig. 7b). In the work of Zhang et al. (2018), similar trend was observed on unsaturated silty clay compacted at a dry density of 1.50 Mg/m^3 while inverse trend was observed at a dry density of 1.75 Mg/m^3 for the same range of temperature (between 0 and -5 °C). Zhang et al. (2018) explained these trends by mentioning two factors: the change of soil density after a freezing-thawing cycle and hysteresis of the soil freezing characteristics curve. In the present work, as the experiments were conducted in a rigid metallic cell, the change of soil density could be ignored. Thus, at a given temperature, volumetric water content was lower on the thawing path (ice content was higher, see more details on the soil freezing characteristic curves of these soils in Vu et al. 2022), which induced a higher thermal conductivity.

Thermal conductivity of unfrozen soils is mostly controlled by water content. The measurements of this study are supplemented by the data from Zhang et al. (2017) not only in the range of high degree of saturation, but also at various porosities. Regarding the plateau of λ in the high range of S_w (higher than 60%), considering that the soils in the present study are dense, it can be explained by a low weighted factor of heat transfer in the pores filled with

468 water and air. In this range of high degree of saturation, it is believed that heat conduction
469 between sand grains through their contact (water) is dominant while the other heat transfer
470 modes, such as conduction in air, radiation in air, convection in air, or vapour diffusion are
471 not significant. λ could decrease only when the amount of water improving the connection
472 between sand grains decreases due to drying process. The later mechanism is observed in Fig.
473 11 where significant decrease of λ in the range of low water degree of saturation follows a
474 nonlinear trend. In addition, for each clay content, the porosity also considerably influences λ.
475 The effect of porosity is also clearly demonstrated by many studies (Chen, 2008; Smits et al.,
476 2010; Tarnawski et al., 2009). The increase of volume of sand grains characterized by the
477 highest λ among the soil components along with decreasing volume of water with low λ
478 contributes to a significant increase of λ of soils.

479 Johansen's model gave a good prediction for unfrozen soils except S15-D1 (fairly good)
480 while De Vries's model gave a fairly good prediction only for S20-D1. Johansen's model,
481 within κ = 8 for all different soils, showed more accurate prediction of measurements than
482 proposed formula of κ based on quartz content in the study of Zhang et al. (2017). The
483 formula could consider the influence of porosity of soils for better prediction.

484 In this study, increasing clay contents increases λ in unfrozen state but an opposite trend is
485 almost observed in frozen state. Considering that the sand skeleton is approximately formed
486 by its optimum structure in terms of limiting pore volume by means of Proctor procedure,
487 adding clay would fill the pores between sand grains. Available space for water is thus
488 reduced by the presence of clay. Due to the replacement of water with λ_w = 0.57 W/(m.K) by
489 clay with higher thermal conductivity λ_c = 2.44 W/(m.K), increasing clay content increases
490 the thermal conductivity at unfrozen state. In frozen state, the opposite trend is almost

observed because of the transformation of liquid water into ice. Actually, while S0-T1 contains pure sand and almost 37% of total soil volume (Table 2) (corresponding to S_r= 0.5% at frozen state as shown in Fig. 8) is filled with ice at frozen state, S20-T1 with 20% clay in solid volume (solids are sand and clay) contains only 21% (corresponding to S_r = 20% and 26% of porosity) of total soil volume filled by ice at frozen state. It is noted that at higher clay contents, more water is kept unfrozen due to the presence of capillary and bound water which could not be frozen at temperatures close to 0 °C. By comparing two extreme cases in this study, it is clear that adding clay in soils not only decreases the available volume for ice in the soils' porosity, but also increases unfrozen water content in frozen state. Consequently, soils with lower clay content have lower λ at unfrozen state but higher λ at frozen state.

6. Conclusions

The variation of clay content (from 0 to 20 %) in sandy soils significantly influences thermal conductivity of soils in both freezing-thawing and drying-wetting processes. Based on the obtained results, some conclusions can be summarized as follows:

- In freezing-thawing process of saturated soils, thermal conductivity in frozen state is considerably higher than that in unfrozen state. The thermal conductivity of frozen soils is higher at a lower unfrozen water content.
- For frozen soil, to provide the same thermal conductivity, volumetric unfrozen water content has to be higher for a higher clay content.
- For unfrozen soil, at a given volumetric water content, thermal conductivity of soils is higher at a higher clay content.

- Johansen's model and De Vries's model cannot predict well thermal conductivity of soil in freezing-thawing process in the studied range of temperature. The models need further improvement for better prediction.
- Johansen's model can predict satisfactorily the thermal conductivity in drying-wetting process but not De Vries's model.

The findings of the present study could be helpful for various engineering applications such as artificial ground freezing or cold regions geo-technologies. In these applications, soils can exist in both unfrozen and frozen states and the effects of clay content on thermal conductivity of sandy soils should be considered when analysing thermal transfers in the ground.

Competing interests

The authors declare there are no competing interests.

Author contribution

Q.H. Vu: Writing – original draft; Data Curation; Formal Analysis; Investigation; Methodology; Visualization. J.M. Pereira: Conceptualization; Project administration; Supervision; Validation; Writing – review & editing. A.M. Tang: Conceptualization; Project administration; Supervision; Validation; Writing – review & editing.

Funding

The authors declare no specific funding for this work.

Data availability

Data generated or analysed during this study are available from the corresponding author upon reasonable request.

References

Abu-Hamdeh, N.H., 2003. Thermal properties of soils as affected by density and water content. Biosyst. Eng. 86, 97–102. https://doi.org/10.1016/S1537-5110(03)00112-0

Abu-Hamdeh, N.H., Reeder, R.C., 2000. Soil thermal conductivity effects of density, moisture, salt concentration, and organic matter. Soil Sci. Soc. Am. J. 64, 1285–1290. https://doi.org/10.2136/sssaj2000.6441285x

Andersland, O.B., Ladanyi, B., 2004. Frozen Ground Engineering. John Wiley & Sons.

Birchak, J.R., Gardner, C.G., Hipp, J.E., Victor, J.M., 1974. High dielectric constant microwave probes for sensing soil moisture. Proc. IEEE 62, 93–98. https://doi.org/10.1109/PROC.1974.9388

Bonales, L.J., Rodriguez, A.C., Sanz, P.D., 2017. Thermal conductivity of ice prepared under different conditions. Int. J. Food Prop. 20, S610–S619. https://doi.org/10.1080/10942912.2017.1306551

Boussaid, K., 2005. Sols intermédiaires pour la modélisation physique : application aux fondations superficielles. École Centrale de Nantes et Université de Nantes.

Bristow, K.L., 1998. Measurement of thermal properties and water content of unsaturated sandy soil using dual-probe heat-pulse probes. Agric. For. Meteorol. 89, 75–84. https://doi.org/10.1016/S0168-1923(97)00065-8

552 Chen, S.X., 2008. Thermal conductivity of sands. Heat Mass Transf. und Stoffuebertragung
553 44, 1241–1246. https://doi.org/10.1007/s00231-007-0357-1

554 Côté, J., Konrad, J.-M., 2005a. A generalized thermal conductivity model for soils and
555 construction materials. Can. Geotech. J. 42, 443–458. https://doi.org/10.1139/T04-106

556 Côté, J., Konrad, J.M., 2005b. Thermal conductivity of base-course materials. Can. Geotech.
557 J. 42, 61–78. https://doi.org/10.1139/t04-081

558 Cui, F.Q., Liu, Z.Y., Chen, J.B., Dong, Y.H., Jin, L., Peng, H., 2020a. Experimental test and
559 prediction model of soil thermal conductivity in permafrost regions. Appl. Sci. 10.
560 https://doi.org/10.3390/app10072476

561 Cui, F.Q., Zhang, W., Liu, Z.Y., Wang, W., Chen, J.B., Jin, L., Peng, H., 2020b. Assessment
562 for thermal conductivity of frozen soil based on nonlinear regression and support vector
563 regression methods. Adv. Civ. Eng. 2020. https://doi.org/10.1155/2020/8898126

564 De Vries, D.A., 1963. Thermal properties of soils. Phys. plant Environ.

565 Farouki, O.T., 1986. Thermal Properties of Soils, Ser. Rock Soil Mech., vol. 11. Trans Tech,
566 Clausthal-Zellerfeld, Ger.

567 Haynes, W.M., 2016. CRC Handbook of Chemistry and Physics, 97th ed. CRC press.

568 He, H., Dyck, M., 2013. Application of multiphase dielectric mixing models for
569 understanding the effective dielectric permittivity of frozen soils. Vadose Zo. J. 12.
570 https://doi.org/10.2136/vzj2012.0060

571 He, H., Flerchinger, G.N., Kojima, Y., Dyck, M., Lv, J., 2021. A review and evaluation of 39

572 thermal conductivity models for frozen soils. Geoderma 382, 114694.
573 https://doi.org/10.1016/j.geoderma.2020.114694

574 Ji, Y., Zhu, K., Lyu, C., Wang, S., Ning, D., Fan, J., Shi, L., 2021. Semiempirical Correlation
575 between P-Wave Velocity and Thermal Conductivity of Frozen Silty Clay Soil. Shock
576 Vib. 2021, 1–7. https://doi.org/10.1155/2021/5533696

577 Johansen, O., 1977. Thermal conductivity of soils. US Army Corps Eng. University of
578 Trondheim, Trondheim, Norway.

579 Johansson, T., 2009. Artificial ground freezing in clayey soils. KTH Architecture and Built
580 Enviroment.

581 Kersten, M.S., 1949. Thermal properties of soils. University of Minnesota.

582 Kim, H.-S., Lee, J.-G., Kang, J.-M., Kim, Y.-S., Hong, S.-S., 2011. Thermal Conductivity of
583 Saturated Unfrozen Kaolinite during Consolidation. J. Eng. Geol. 21, 157–162.

584 Lawson, A.W., Lowell, R., Jain, A.L., 1959. Thermal Conductivity of Water at High
585 Pressures. J. Chem. Phys. 30, 643–647. https://doi.org/10.1063/1.1730024

586 Li, Z., Chen, J., Sugimoto, M., 2020. Pulsed NMR Measurements of Unfrozen Water Content
587 in Partially Frozen Soil. J. Cold Reg. Eng. 34, 04020013.
588 https://doi.org/10.1061/(ASCE)CR.1943-5495.0000220

589 Lu, Y., Yu, W., Hu, D., Liu, W., 2018. Experimental study on the thermal conductivity of
590 aeolian sand from the Tibetan Plateau. Cold Reg. Sci. Technol. 146, 1–8.
591 https://doi.org/10.1016/j.coldregions.2017.11.006

Mickley, A.S., 1951. The Thermal Conductivity of Moist Soil. Trans. Am. Inst. Electr. Eng. 70, 1789–1797. https://doi.org/10.1109/T-AIEE.1951.5060631

Nagare, R.M., Schincariol, R.A., Quinton, W.L., Hayashi, M., 2011. Laboratory calibration of time domain reflectometry to determine moisture content in undisturbed peat samples. Eur. J. Soil Sci. 62, 505–515. https://doi.org/10.1111/j.1365-2389.2011.01351.x

Nguyen, V.T., Heindl, H., Pereira, J.M., Tang, A.M., Frost, J.D., 2017. Water retention and thermal conductivity of a natural unsaturated loess. Géotechnique Lett. 7, 286–291. https://doi.org/10.1680/jgele.17.00037

Penner, E., 1970. Thermal conductivity of frozen soils. Can. J. Earth Sci. 7, 982–987. https://doi.org/10.1139/e70-091

Penner, E., Johnston, G.H., Goodrich, L.E., 1975. Thermal conductivity laboratory studies of some Mackenzie Highway Soils. Can. Geotech. J. 12, 271–288.

Roth, K., Schulin, R., Fluhler, H., Attinger, W., 1990. Calibration of time domain reflectometry for water content measurement using a composite dielectric approach. Water Resour. Res. 26, 2267–2273.

Schafer, H., Beier, N., 2020. Estimating soil-water characteristic curve from soil-freezing characteristic curve for mine waste tailings using time domain reflectometry. Can. Geotech. J. 57, 73–84. https://doi.org/10.1139/cgj-2018-0145

Sepaskhah, A.R., Boersma, L., 1979. Thermal Conductivity of Soils as a Function of Temperature and Water Content. Soil Sci. Soc. Am. J. 43, 439–444. https://doi.org/10.2136/sssaj1979.03615995004300030003x

Slack, G.A., 1980. Thermal conductivity of ice. Phys. Reveiw B 22, 3065.

Smith, M.W., Tice, A.R., 1988. Measurement of the unfrozen water content of soils: comparison of NMR and TDR methods, Cold Regions Reserach and Engineering Laboratory. Hanover.

Smits, K.M., Sakaki, T., Limsuwat, A., Illangasekare, T.H., 2010. Thermal Conductivity of Sands under Varying Moisture and Porosity in Drainage–Wetting Cycles. Vadose Zo. J. 9, 172. https://doi.org/10.2136/vzj2009.0095

Spaans, E.J. a, Baker, J.M., 1995. Examining the use of time domain refiectometry for measuring liquid water content in frozen soil. Water Resour. Res. 31, 2917–2925. https://doi.org/10.1029/95WR02769

Stähli, M., Stadler, D., 1997. Measurement of water and solute dynamics in freezing soil columns with time domain reflectometry. J. Hydrol. 195, 352–369. https://doi.org/10.1016/S0022-1694(96)03227-1

Tang, A.M., Cui, Y.J., Le, T.T., 2008. A study on the thermal conductivity of compacted bentonites. Appl. Clay Sci. 41, 181–189. https://doi.org/10.1016/j.clay.2007.11.001

Tarnawski, V.R., Leong, W.H., 2000. Thermal conductivity of soils at very low moisture content and moderate temperatures. Transp. Porous Media 41, 137–147. https://doi.org/10.1023/A:1006738727206

Tarnawski, V.R., Momose, T., Leong, W.H., Bovesecchi, G., Coppa, P., 2009. Thermal Conductivity of Standard Sands. Part I. Dry-State Conditions. Int. J. Thermophys. 30, 949–968. https://doi.org/10.1007/s10765-009-0596-0

Tarnawski, V.R., Momose, T., McCombie, M.L., Leong, W.H., 2015. Canadian Field Soils III. Thermal-Conductivity Data and Modeling. Int. J. Thermophys. 36, 119–156. https://doi.org/10.1007/s10765-014-1793-z

Tarnawski, V.R., Wagner, B., 1992. A new computerized approach to estimating the thermal properties of unfrozen soils. Can. Geotech. J. 29, 714–720. https://doi.org/10.1139/t92-079

Tian, H., Wei, C., Wei, H., Zhou, J., 2014. Freezing and thawing characteristics of frozen soils: Bound water content and hysteresis phenomenon. Cold Reg. Sci. Technol. 103, 74–81. https://doi.org/10.1016/j.coldregions.2014.03.007

Tian, Z., Lu, Y., Horton, R., Ren, T., 2016. A simplified de Vries-based model to estimate thermal conductivity of unfrozen and frozen soil. Eur. J. Soil Sci. 67, 564–572. https://doi.org/10.1111/ejss.12366

Tian, Z., Ren, T., Kojima, Y., Lu, Y., Horton, R., Heitman, J.L., 2017. An improved thermo-time domain reflectometry method for determination of ice contents in partially frozen soils. J. Hydrol. 555, 786–796. https://doi.org/10.1016/j.jhydrol.2017.10.055

Tice, A.R., Anderson, D.M., Banin, A., 1976. The prediction of unfrozen water contents in frozen soils from liquid limit determinations 76.

Topp, G.C., Davis, J.L., Annan, A.P., 1980. Electromagnetic determination of soil water content: Measurements in coaxial transmission lines. Water Resour. Reserch 16, 574–582.

Vieira, A., Maranha, J.R., Lapa, J., Figueiredo, A., 2019. Some aspects of measurement of

655 sand thermal conductivity from laboratory tests. Proc. XVII ECSMGE.
656 https://doi.org/10.32075/17ECSMGE-2019-0541

657 Vu, Q.H., Pereira, J.M., Tang, A.M., 2022. Effect of fines content on soil freezing
658 characteristic curve of sandy soils. Acta Geotech. 17, 4921–4933.
659 https://doi.org/10.1007/s11440-022-01672-9

660 Wang, J., He, H., Dyck, M., Lv, J., 2020. A review and evaluation of predictive models for
661 thermal conductivity of sands at full water content range. Energies 13.
662 https://doi.org/10.3390/en13051083

663 Watanabe, K., Wake, T., 2009. Measurement of unfrozen water content and relative
664 permittivity of frozen unsaturated soil using NMR and TDR. Cold Reg. Sci. Technol. 59,
665 34–41. https://doi.org/10.1016/j.coldregions.2009.05.011

666 Wraith, J.M., Or, D., 1999. Temperature effects on soil bulk dielectric permittivity measured
667 by time domain refiectometry: Experimental evidence and hypothesis development.
668 Water Resour. Res. 35, 361–369.

669 Yan, H., He, H., Dyck, M., Jin, H., Li, M., Si, B., Lv, J., 2019. A generalized model for
670 estimating effective soil thermal conductivity based on the Kasubuchi algorithm.
671 Geoderma 353, 227–242. https://doi.org/10.1016/j.geoderma.2019.06.031

672 Zhang, M., Lu, J., Lai, Y., Zhang, X., 2018. Variation of the thermal conductivity of a silty
673 clay during a freezing-thawing process. Int. J. Heat Mass Transf. 124, 1059–1067.
674 https://doi.org/10.1016/j.ijheatmasstransfer.2018.02.118

675 Zhang, M., Zhang, X., Lai, Y., Lu, J., Wang, C., 2020. Variations of the temperatures and

volumetric unfrozen water contents of fine-grained soils during a freezing–thawing process. Acta Geotech. 15, 595–601. https://doi.org/10.1007/s11440-018-0720-z

Zhang, N., Yu, X., Pradhan, A., Puppala, A.J., 2017. A new generalized soil thermal conductivity model for sand–kaolin clay mixtures using thermo-time domain reflectometry probe test. Acta Geotech. 12, 739–752. https://doi.org/10.1007/s11440-016-0506-0

Zhang, N., Yu, X., Pradhan, A., Puppala, A.J., 2015. Effects of particle size and fines content on thermal conductivity of Quartz sands. Transp. Res. Rec. 2510, 36–43. https://doi.org/10.3141/2510-05

Zhao, X., Zhou, G., Jiang, X., 2019. Measurement of thermal conductivity for frozen soil at temperatures close to 0 °C. Meas. J. Int. Meas. Confed. 140, 504–510. https://doi.org/10.1016/j.measurement.2019.03.069

Zhao, Y., Si, B., 2019. Thermal properties of sandy and peat soils under unfrozen and frozen conditions. Soil Tillage Res. 189, 64–72. https://doi.org/10.1016/j.still.2018.12.026

Zhou, X., Zhou, J., Kinzelbach, W., Stauffer, F., 2014. Simultaneous measurement of unfrozen water content and ice content in frozen soil using gamma ray attenuation and TDR. Water Resour. Res. 50, 9630–9655. https://doi.org/10.1002/2014WR015640

Table captions

Table 1. Physical properties of Speswhite Kaolin clay and Fontainebleau sand (Boussaid, 2005).

Table 2. Physical properties of soils in freezing-thawing (T1) and drying-wetting (D1) experiments.

Table 3. Properties of sensors used in freezing-thawing and drying-wetting experiments.

721

722 **Figure captions**

723 Fig. 1 Grain size distribution curves.

724 Fig. 2. Setup for freezing-thawing experiment: (1) Temperature-controlled bath; (2) Soil
725 specimen; (3) Temperature control system; (4) Heat transfer liquid (30% ethylene glycol +
726 70% water); (5) Metallic cylindrical cell; (6) Insulating cover; (7) Temperature sensor; (8)
727 Tensiometer; (9) Soil water content sensor; (10) Thermal conductivity probe; (11) Data
728 logging system.

729 Fig. 3. Setup of drying-wetting experiment: (1) Soil; (2) Metallic cylindrical cell; (3)
730 Insulating cover; (4) Tensiometer; (5) Thermal conductivity probe; (6) Soil water content
731 sensor; (7) Data logging system.

732 Fig. 4. Temporal variation of temperature, unfrozen volumetric water content and thermal
733 conductivity during test S10-T1.

734 Fig. 5. Relationships between thermal conductivity, temperature and volumetric unfrozen
735 water content of test S10-T1.

736 Fig. 6. Thermal conductivity versus temperature for all freezing-thawing experiments.

737 Fig. 7. Thermal conductivity versus (a) volumetric unfrozen water content and (b)temperature
738 for all freezing-thawing experiments.

739 Fig. 8. Experimental results and models' prediction for thermal conductivity versus water
740 degree of saturation: (a) S0-T1; (b) S05-T1; (c) S10-T1; (d) S15-T1; (e) S20-T1.

741 Fig. 9. Volumetric water content and thermal conductivity of unfrozen soils in wetting drying
742 process of S10-D1.

743 Fig. 10. Thermal conductivity versus water degree of saturation for all drying-wetting
744 experiments.

745 Fig. 11. Experimental results (obtained in this study and in the study of N. Zhang et al., 2017)
746 and models prediction for thermal conductivity versus degree of saturation: (a) S0; (b) S5; (c)
747 S10; (d) S15; (e) S20.

748 Fig. 12. Configuration of soil media in (a) unfrozen saturated state, (b) frozen saturated state
749 and (c) unfrozen unsaturated state.

750